Symmetry-Resolved Two-Magnon Excitations in a Strong Spin-Orbit-Coupled Bilayer Antiferromagnet

Siwen Li,[1] Elizabeth Drueke,[1] Zach Porter,[2] Wencan Jin,[1,‡] Zhengguang Lu,[3,4] Dmitry Smirnov,[3] Roberto Merlin,[1] Stephen D. Wilson,[2] Kai Sun,[1,*] and Liuyan Zhao[1,†]

[1]*Department of Physics, University of Michigan, Ann Arbor, Michigan 48109, USA*
[2]*Materials Department, University of California, Santa Barbara, California 93106, USA*
[3]*National High Magnetic Field Laboratory, Tallahassee, Florida 32310, USA*
[4]*Department of Physics, Florida State University, Tallahassee, Florida 32310, USA*

(Received 25 March 2020; accepted 29 July 2020; published 20 August 2020)

We used a combination of polarized Raman spectroscopy and spin wave calculations to study magnetic excitations in the strong spin-orbit-coupled bilayer perovskite antiferromagnet $Sr_3Ir_2O_7$. We observed two broad Raman features at ~800 and ~1400 cm^{-1} arising from magnetic excitations. Unconventionally, the ~800 cm^{-1} feature is fully symmetric (A_{1g}) with respect to the underlying tetragonal (D_{4h}) crystal lattice which, together with its broad line shape, definitively rules out the possibility of a single magnon excitation as its origin. In contrast, the ~1400 cm^{-1} feature shows up in both the A_{1g} and B_{2g} channels. From spin wave and two-magnon scattering cross-section calculations of a tetragonal bilayer antiferromagnet, we identified the ~800 cm^{-1} (1400 cm^{-1}) feature as two-magnon excitations with pairs of magnons from the zone-center Γ point (zone-boundary van Hove singularity X point). We further found that this zone-center two-magnon scattering is unique to bilayer perovskite magnets which host an optical branch in addition to the acoustic branch, as compared to their single layer counterparts. This zone-center two-magnon mode is distinct in symmetry from the time-reversal symmetry broken "spin wave gap" and "phase mode" proposed to explain the ~92 meV (742 cm^{-1}) gap in resonant inelastic x-ray spectroscopy magnetic excitation spectra of $Sr_3Ir_2O_7$.

DOI: 10.1103/PhysRevLett.125.087202

Bilayer antiferromagnets (AFMs) of square lattice are of particular interest because they are predicted to realize a quantum phase transition from a conventional AFM phase to a long-sought quantum dimer phase [1–4] across a critical ratio ($r_c = 2.522$) of nearest-neighbor interlayer (J_c) to intralayer (J) exchange coupling [5,6]. Until very recently, experimental explorations of such bilayer AFM physics have been limited to materials with very weak spin-orbit-coupling (SOC), such as AFM bilayer cuprates [7,8], manganese fluoride [9], and ruthenates [10] of perovskite structures, where J_c is orders of magnitude smaller than J, and thus their magnetic excitations are of a simple perturbation from their single layer counterparts. The recent success in growing high-quality $5d$ perovskite iridates with strong SOC makes it possible to have comparable J_c and J and result in unconventional magnetic properties.

The bilayer perovskite iridate $Sr_3Ir_2O_7$ exhibits a strong SOC-assisted Mott insulating electronic ground state [11–17] and G-type AFM order [Fig. 1(a)] [18–22]. Its $J_{\text{eff}} = 1/2$ magnetic moment, which results from equal contributions from the three t_{2g} orbitals, d_{xy}, d_{xz}, and d_{yz}, makes it possible for J_c to be on the same order of magnitude as J [Figs. 1(b) and 1(c)]. The magnetic excitation spectrum of this compound, previously measured by resonant inelastic x-ray spectroscopy (RIXS), shows a prominent feature ascribed to a "spin gap" of ~92 meV (742 cm^{-1}) [23]. This spin gap is much greater than the Néel temperature energy $T_N = 285$ K (~200 cm^{-1}) [24] and the magnetic dispersion bandwidth ~70 meV (565 cm^{-1}) [23], and is even comparable to the Mott charge gap of ~100 meV (807 cm^{-1}) [13,14,16]. As such, the magnetism in $Sr_3Ir_2O_7$ is in seemingly stark contrast to that of its single layer counterpart Sr_2IrO_4, a SOC cuprate analogue [25–29] whose magnetism is well described by the nearly isotropic Heisenberg spin model [30].

Two distinct theory approaches have been proposed to explain this anomalously giant spin gap in the RIXS data, namely, the spin wave theory [23,31] and the bond operator approach [32,33]. In the spin wave theory, the giant spin gap is treated as the energy cost for exciting a single zone-center magnon, which suggests an exceptionally large magnetic exchange anisotropy [23,31]. In the bond operator approach, this "gap" is ascribed to the energy of a transverse magnetic mode (i.e., the phase mode), which is also a single-spin scattering process [32]. Until now, the nature of this spin gap in $Sr_3Ir_2O_7$ has remained elusive, except that both approaches suggest it originates from a time-reversal symmetry breaking single-spin process and requires strong magnetic anisotropy. The former requires

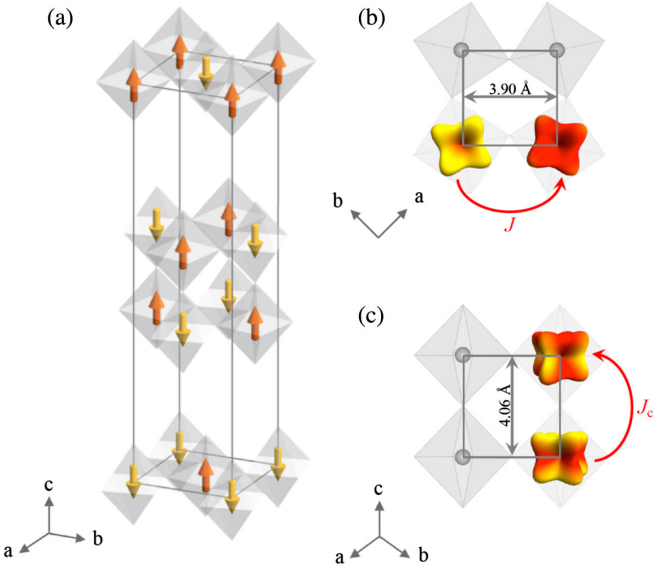

FIG. 1. Crystalline and magnetic structures of $Sr_3Ir_2O_7$. (a) The expanded unit cell for the bilayer AFM $Sr_3Ir_2O_7$, where gray octahedra are the oxygen octahedra, gray spheres are the Ir atoms, and orange and yellow arrows are $J_{\text{eff}} = \pm 1/2$ magnetic moments. (b) Top view of a layer of IrO cages, where J stands for the nearest-neighbor intralayer exchange coupling. (c) Side view of two layers of IrO cages within a bilayer, where J_c stands for the nearest-neighbor interlayer exchange coupling. a, b, and c are crystal axes. The yellow-red colored patterns in (b) and (c) are for the $J_{\text{eff}} = \pm 1/2$ wave functions.

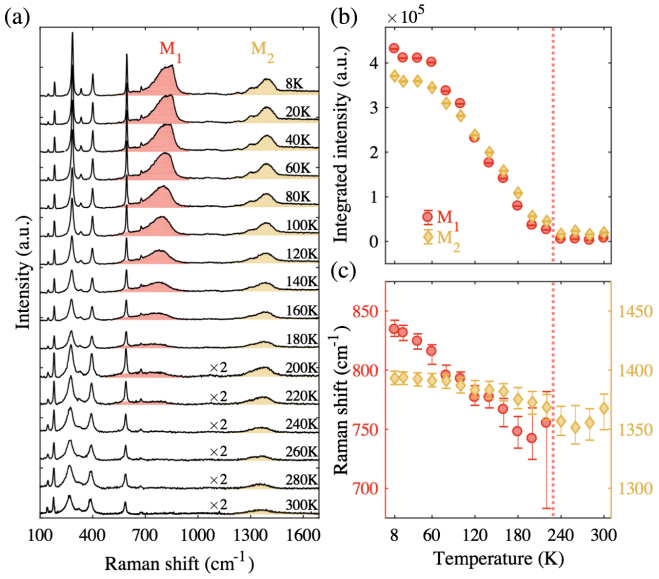

FIG. 2. Temperature dependent magnetic Raman spectra of $Sr_3Ir_2O_7$. (a) Raman spectra taken over a temperature range from 300 down to 8 K with linearly polarized incident (whose polarization is at about 45° from crystal axis (a) and unpolarized scattered light, where the spectra above 200 K are multiplied by a factor of 2. These spectra are offset vertically for clarity. M_1 and M_2 label the two broad continuums shaded in red and yellow, respectively. (b) Temperature dependence of the extracted peak intensities for M_1 and M_2. (c) Temperature dependence of the extracted central frequencies for M_1 and M_2. The error bars in (b) and (c) are defined by one standard error for the extracted parameters.

an in-depth examination as selection rules in the x-ray wavelengths is much less known than those in the optical wavelengths [34], while the latter is in direct contrast to the weak magnetic anisotropy and its associated nearly zero spin gap in the single layer counterpart Sr_2IrO_4.

The spin gap in $Sr_3Ir_2O_7$ has so far only been detected experimentally by RIXS, as the strong neutron absorption and small crystal size of iridates preclude inelastic neutron scattering as an efficient probe. Optical Raman scattering is another well-known probe for magnetic excitations in addition to phononic and electronic ones [35]. So far, Raman spectra of bilayer perovskite iridate have not revealed a signature that matches the spin gap [36], but show a broad continuum feature centered at ~175 meV (1410 cm^{-1}) of B_{2g} symmetry in both Sr_2IrO_4 and $Sr_3Ir_2O_7$ [36] arising from zone-boundary two-magnon scattering in a way similar to that in cuprates.

Here, we perform magnetic Raman measurements including symmetry channels beyond B_{2g}. Our temperature dependent (polarized) Raman measurements were performed in a normal incidence and backscattering geometry, the incident excitation being a cw laser with a wavelength of 532 nm (514 nm) that is focused down to ~3 μm (30 μm) in diameter at the sample site at a power of <80 μW(<1.5 mW) whereas the scattered light being analyzed by a Princeton Instrument TriVista spectrometer (a triple grating Dilor XY spectrometer).

Figure 2(a) displays temperature dependent Raman spectra taken across T_N using a configuration with linearly polarized incident and unpolarized scattered light to collect as many features as possible. Three types of salient features can be immediately seen from these spectra, the sharp peaks below 700 cm^{-1} present at all temperatures, the broad feature at ~800 cm^{-1} only appearing at low temperatures (M_1, shaded in red), and the other continuum centered at ~1400 cm^{-1} persisting up to room temperature (M_2, shaded in yellow). The sharp peaks are the Raman active optical phonons of $Sr_3Ir_2O_7$ whose frequencies are consistent with those in a previous report [35,36]. M_2 at low temperature exhibits a complex structure with a main broad peak at ~1400 cm^{-1}, two shoulders at ~1230 and 1300 cm^{-1}, and a long tail extending beyond 1700 cm^{-1}. This feature has been attributed to zone-boundary two-magnon scattering, whose line shape differs from that in Ref. [36] due to the different photon excitation energies. A similar feature at a similar energy was observed in the single layer counterpart Sr_2IrO_4, confirming that the pairs of magnons participating in this two-magnon scattering process come mainly from the in-plane Brillouin zone boundary. Finally, M_1, unlike M_2, is absent in Sr_2IrO_4 [36] and is the focus of this work.

We now proceed to establish the magnetic origin of M_1. This expectation of a magnetic origin is well motivated by the energy scale, which matches the giant spin gap at ~92 meV [23,32]. Further, the temperature dependence of the M_1 peak intensity in Fig. 2(b) that closely mimics that of M_2, reveals an onset temperature of $T_{N'} = 230$ K that coincides with the onset of the AFM order in resonant x-ray diffraction measurements [20]. In addition, the M_1 central frequency blueshifts by ~100 cm^{-1} since its onset $T_{N'}$ [Fig. 2(c)], indicating that M_1 results from soft modes below $T_{N'}$. The only other possible sources of origin are phononic and electronic ones. Its greater than 100 cm^{-1} linewidth precludes the possibility that it is due to a first-order single optical phonon excitation, and it is unlikely to result from any multiphonon scattering processes because of its high intensity comparable to that of any Raman active phonons in $Sr_3Ir_2O_7$. An electronic origin can also be ruled out because, although the energy scale of ~800 cm^{-1} is close to the charge gap in $Sr_3Ir_2O_7$, ~100 meV [13,14,16], this charge gap is known to be an indirect gap and should not be detected by the zero-momentum optical Raman scattering. Therefore, based on the exclusion of the phononic and electronic origins, as well as the agreement of its energy and onset temperature with those of the AFM order, we assign this broad continuum M_1 in $Sr_3Ir_2O_7$ arising from magnetic excitations.

Despite the fact that M_1 has the same energy as the giant spin gap from RIXS, its nature has yet to be resolved. We have performed polarized Raman spectroscopy measurements in all four selection rule channels of the underlying D_{4h} crystal lattice (Fig. 3) namely, aa, $a'a'$, ab, and $a'b'$ (insets of Fig. 3), corresponding to the parallel polarizations between the incident (solid arrow) and scattered (dashed arrow) polarizations aligning along and 45° rotated from a axis and their counterparts in the crossed channels. As expected, the optical phonons show up in only one of the A_{1g}, B_{2g}, and B_{1g} symmetry channels [36], confirming the D_{4h} tetragonal lattice point group. In contrast to the phonons, M_2 appears not only in the B_{2g} channel as reported in Ref. [36], but also in the A_{1g} channel. This is, however, not surprising for zone-boundary two-magnon scattering, as similar observations were previously reported in cuprates [37]. Remarkably, M_1 can only be observed in the A_{1g} channel, showing that the magnetic excitations responsible for M_1 preserve all symmetry operations of the underlying D_{4h} lattice point group. It is known that any single-spin excitations definitely break either time reversal symmetry, corresponding to magnetism-induced circular dichroism and birefringence, or lattice point symmetries, resulting in magnetism-induced linear dichroism and birefringence [38]. Thus, the full symmetry of M_1, together with its broad line shape, clearly rules out the possibility that it is due to single-spin excitations assigned in a recent Raman study of $Sr_3Ir_2O_7$ [39]. In the following, we show that it originates from two-spin excitations.

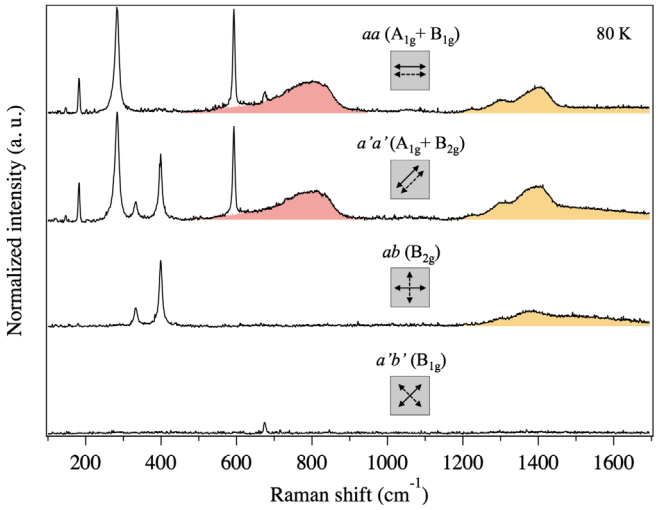

FIG. 3. Symmetry selection rules for the magnetic excitations in $Sr_3Ir_2O_7$. Raman spectra were taken at 80 K in four polarization channels: aa, $a'a'$, ab, and $a'b'$. The insets indicate the polarization channels and the selected symmetry modes under the D_{4h} point group.

We performed two-magnon scattering calculations based on the spin wave theory of a SOC bilayer Heisenberg AFM. The motivation is threefold. First, it is consistent with the fact that the broad continuum at ~1400 cm^{-1}, zone-boundary two-magnon scattering, is present in the Raman spectra of $Sr_3Ir_2O_7$ [36]. Second, it is corroborated by a recent study showing that the in-plane Ir-O-Ir length of 3.90 Å is notably smaller than the out-of-plane length of 4.06 Å [Figs. 1(b) and 1(c)] [40], suggesting that J_c/J would be significantly smaller than the quantum critical point at $r_c = 2.522$ when the orbital character of $J_{\text{eff}} = 1/2$ is nearly isotropic. Finally, the choice of this model is self-consistent in that it gives $r = 0.19$ and an intralayer exchange coupling strength in $Sr_3Ir_2O_7$ comparable to that in Sr_2IrO_4. We adopt a leading order Loudon-Fleury scattering Hamiltonian, $H_{\text{LF}} = \alpha \sum_{\langle i,j \rangle} (\vec{E}_I \cdot \vec{\sigma}_{ij})(\vec{E}_S \cdot \vec{\sigma}_{ij}) \vec{S}_i \cdot \vec{S}_j$, where $\vec{E}_I$ and $\vec{E}_S$ are the incident and scattered electric fields, respectively, and $\vec{\sigma}_{ij}$ is the unit vector connecting sites i and j [38]. We examine both a simplified spin Hamiltonian with only nearest-neighbor AFM exchange couplings and a more realistic one considering up to the third-nearest-neighbor coupling [30] and a dipolelike spin exchange for strong SOC [41]. Through their comparisons, we find that the interpretation of the fully symmetric M_1 as zone-center two-magnon scattering is robust in that it is independent of the choice of spin Hamiltonian.

We begin with a simple spin model with only nearest-neighbor intralayer (J) and interlayer (J_c) coupling to grasp the necessary elements for understanding M_1. Because the bilayer doubles the number of degrees of freedom, there are two sets of doubly degenerate magnon bands. At the Γ point, one set of doubly degenerate magnon bands remains

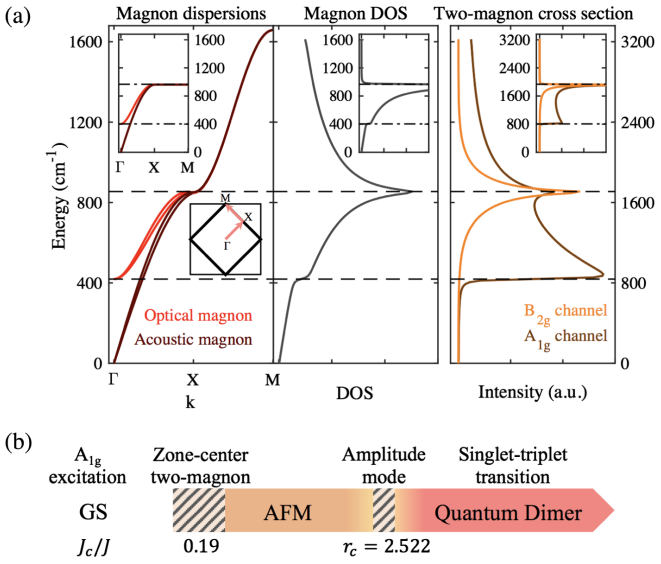

FIG. 4. Theoretical calculations for magnetic excitations in $Sr_3Ir_2O_7$. (a) Calculated magnon band dispersions along the high symmetry cut in the momentum space Γ-X-M (left), magnon DOS (middle), and two-magnon scattering cross section in the A_{1g} and B_{2g} channels (right) under the nearest-neighbor (inset) and the longer-range (main panels) exchange coupling approximation. The magnon dispersions and DOS share the same vertical axis (left side axis) while the two-magnon cross section has its own vertical axis (right side axis). (b) Schematics to illustrate the magnetic ground states and two-spin excitations as a function of $r = J_c/J$.

gapless with a linear dispersion (acoustic magnon branch), similar to that of Sr_2IrO_4 [30], and importantly, the other set is gapped by a finite energy (optical magnon branch), absent in Sr_2IrO_4 [Fig. 4(a) inset, left]. Consequently, the magnon density of states (DOS) has a steplike jump at this gap energy [Fig. 4(a) inset, middle], and an interlayer onsite Loudon-Fleury scattering Hamiltonian leads to an observable feature of zone-center two-magnon excitations in the Raman spectra [Fig. 4(a) inset, right]. Because the Γ point is the highest symmetry point in the momentum space that preserves all of the symmetry operations of the crystal lattice, the zone-center two-magnon scattering feature should be fully symmetric with respect to the lattice [42]. Therefore, M_1 can be understood as two-magnon excitations with pairs of magnons from the optical branch at the Γ point, with calculated energy $4\sqrt{JJ_c}$ [42]. Meanwhile, we note the difference in M_1 line shape between the experimental and calculated spectra that experimental data show a long tail whereas the calculation depicts a sharp drop at the lower-energy side of M_1. This difference arises mainly from two factors omitted in the calculations but present in experiment, the thermal broadening effect that is expected to impact more on the lower-energy side for a broad feature like M_1 and the magnon-magnon interactions that could create two-magnon states at energies lower than twice optical magnon gap.

We also confirm that M_2 originates from two-magnon excitations at the zone-boundary. The fact that the two magnon bands are degenerate and dispersionless along X-M [Fig. 4(a) inset, left] leads to a divergent DOS at every momentum point along X-M [Fig. 4(a) inset, middle], resulting in zone-boundary two-magnon scattering feature prominent in Raman spectra of bilayer AFMs [Fig. 4(a) inset, right], similar as in the case of cuprates [43]. Because of divergent DOS, quantum corrections to account for magnon interactions are needed in computing two-magnon scattering, making the actual energy of the two-magnon feature reduced by a factor of 0.73 [44] from the directly computed value of $2\sqrt{J(4J+2J_c)}$. Note that this correction factor of 0.73 is confirmed appropriate in Sr_2IrO_4 as the ratio of its two-magnon energy in Raman (160 meV [36]) to twice its single magnon energy at X point (220 meV $= 2 \times 110$ meV [30]) is $\sim$0.73. Comparing these calculated results with our experimental values of $\sim$800 and $\sim$1400 cm^{-1}, we obtain estimated values of $J = 458$ and $J_c = 87$ cm^{-1}. The value of $r = J_c/J = 0.19$ is much smaller than the quantum critical point $r_c = 2.522$, which in turn corroborates our choice of the spin wave theory in interpreting the magnetic excitations in $Sr_3Ir_2O_7$.

In reality, a more sophisticated spin Hamiltonian is needed to describe $Sr_3Ir_2O_7$ magnetism [41], including interlayer exchange coupling ($J_c = 91$ cm^{-1} optimized in this work), first, second, and third nearest-neighbor intralayer exchange coupling ($J = 484$, $J_2 = -161$, and $J_3 = 121$ cm^{-1} directly adopted from Ref. [30] for Sr_2IrO_4) and SOC induced dipolelike exchange coupling [$H_{\mathrm{SOC}} = \Delta \sum_{i,i',n} (\vec{S}_{i,n} \cdot \vec{\sigma}_2)(\vec{S}_{i',n} \cdot \vec{\sigma}_2)$ with $\Delta = 16$ cm^{-1} based on Ref. [41] for Sr_2IrO_4] to account for the magnon dispersion along X-M [Fig. 4(a), left]. The optimized J_c of 91 cm^{-1} here is very close to that of 87 cm^{-1} from the simple spin Hamiltonian above, confirming the robustness of its value, as well as the choice of spin wave theory, in $Sr_3Ir_2O_7$. Furthermore, even when these terms in addition to J and J_c are taken into account, the physics for M_1 remains exactly the same as in the simple model [Fig. 4(a)] because the defining feature is the presence of the gapped optical branch at the zone-center and has nothing to do with magnons at the zone boundary. In contrast, the physics for M_2 requires an extension of the simple model because now the divergent DOS appears only at the van Hove singularity point X [Fig. 4(a), middle] and cannot be accessed by any nearest-neighbor two-spin scattering Hamiltonian [42], which therefore requires the next-nearest-neighbor two-spin flip processes in the Loudon-Fleury scattering formalism. Such processes, however, violate spin conservation in AFMs by flipping two spins with the same orientation to the opposite direction, and thus, are only allowed in AFMs with strong SOC that breaks the SU(2) spin rotational symmetry. In iridates, strong SOC indeed exists and manifests itself in the spin Hamiltonian through a

dipolelike spin exchange term, which is known to produce spin anisotropy and determine the orientation of AFM magnetic moments [41]. Our calculations reveal that even a very small amount of SOC in the scattering Hamiltonian can lead to the observation of zone-boundary two-magnon excitations from the X point in both the A_{1g} and B_{2g} channels [Fig. 4(a), right] [42].

We further discuss the relationship between M_1 and the intriguing amplitude mode near the quantum critical point $r_c = 2.522$ [Fig. 4(b)]. On the one hand, the zone-center two-magnon excitations and the amplitude mode (i.e., Higgs mode) share exactly the same symmetries and can both be characterized, to the leading order, by an interlayer on-site Loudon-Fleury scattering Hamiltonian [6]. The amplitude mode is in general damped by other low-energy excitations, and therefore, results in a broad line shape similar to that of the zone-center two-magnon excitations. These similarities imply that they are simply two different manifestations of the same heavily damped object without a well-defined boundary to distinguish the two. On the other hand, the amplitude mode and the zone-center two-magnon excitation do happen at different r in a bilayer AFM. The zone-center two-magnon excitations only become visible when J_c is weak compared with J (i.e., well below r_c) and dissolves into the background upon increased J_c. In recent numeric studies [6], the amplitude mode is only underdamped and well defined in a very small window near the quantum critical point r_c, and neither amplitude mode nor zone-center two-magnon mode appears for intermediate r between the two regimes.

Finally, we comment on the relationship between the zone-center two-magnon excitations in the Raman spectra and the giant spin gap in the RIXS spectra in Refs. [23,32]. It is apparent that these two features have nearly the same energy, but sharply distinct symmetries. A trivial explanation could be that they are two different but energetically degenerate objects that happen to be captured by Raman and RIXS in a complementary way. A less trivial possibility could be that they are indeed one and the same object, which would suggest a reconsideration of the conventional selection rules. Optical Raman selection rules are well defined based on the electric dipole approximation, which is justified in the fact that optical wavelengths are much larger than lattice constants and is further confirmed by the correct selection rules for the phonon modes. Resonant x-ray spectroscopy selection rules are less well defined because of contributions from higher order multipolar transitions in addition to the electric dipole transitions [34]. In the electric-dipole channel, the polarization of the incoming x ray rotating to a perpendicular polarization in the scattered x ray reflects time-reversal-symmetry-breaking excitations, whereas in the electric-quadrupole or higher multipole channels, such a rotation is naturally allowed even for excitations of the A_{1g} symmetry, as the case for the RIXS on the spin gap of $Sr_3Ir_2O_7$.

L. Z. acknowledges support by National Science Foundation CAREER Grant No. DMR-1749774. K. S. acknowledges support by National Science Foundation Grant No. NSF-EFMA-1741618. S. D. W. acknowledges support by National Science Foundation Grant No. DMR-1905801 and by Army Research Office Grant No. W19NF-16-1-0361 (Z. P.). E. D. acknowledges support by the National Science Foundation Graduate Research Fellowship Program under Grant No. DGE-1256260. The work done at the National High Magnetic Field Laboratory is supported by National Science Foundation Grant No. DMR-1644779.

*Corresponding author.
sunkai@umich.edu
†Corresponding author.
lyzhao@umich.edu
‡Present address: Department of Physics, Auburn University 380 Duncan Drive, Auburn, AL 36849, USA.

[1] A. V. Chubukov and D. K. Morr, Phys. Rev. B **52**, 3521 (1995).
[2] A. W. Sandvik, A. V. Chubukov, and S. Sachdev, Phys. Rev. B **51**, 16483 (1995).
[3] C. N. A. van Duin and J. Zaanen, Phys. Rev. Lett. **78**, 3019 (1997).
[4] V. N. Kotov, O. Sushkov, W. Zheng, and J. Oitmaa, Phys. Rev. Lett. **80**, 5790 (1998).
[5] L. Wang, K. S. D. Beach, and A. W. Sandvik, Phys. Rev. B **73**, 014431 (2006).
[6] M. Lohöfer, T. Coletta, D. G. Joshi, F. F. Assaad, M. Vojta, S. Wessel, and F. Mila, Phys. Rev. B **92**, 245137 (2015).
[7] A. J. Millis and H. Monien, Phys. Rev. B **50**, 16606 (1994).
[8] D. Reznik, P. Bourges, H. F. Fong, L. P. Regnault, J. Bossy, C. Vettier, D. L. Milius, I. A. Aksay, and B. Keimer, Phys. Rev. B **53**, R14741 (1996).
[9] C. van Uijen, A. Arts, and H. de Wijn, Solid State Commun. **47**, 455 (1983).
[10] X. Ke, T. Hong, J. Peng, S. E. Nagler, G. E. Granroth, M. D. Lumsden, and Z. Q. Mao, Phys. Rev. B **84**, 014422 (2011).
[11] S. J. Moon *et al.*, Phys. Rev. Lett. **101**, 226402 (2008).
[12] B. M. Wojek, M. H. Berntsen, S. Boseggia, A. T. Boothroyd, D. Prabhakaran, D. F. McMorrow, H. M. Rønnow, J. Chang, and O. Tjernberg, J. Phys. Condens. Matter **24**, 415602 (2012).
[13] Y. Okada *et al.*, Nat. Mater. **12**, 707 (2013).
[14] Q. Wang, Y. Cao, J. A. Waugh, S. R. Park, T. F. Qi, O. B. Korneta, G. Cao, and D. S. Dessau, Phys. Rev. B **87**, 245109 (2013).
[15] A. de la Torre, E. C. Hunter, A. Subedi, S. McKeown Walker, A. Tamai, T. K. Kim, M. Hoesch, R. S. Perry, A. Georges, and F. Baumberger, Phys. Rev. Lett. **113**, 256402 (2014).
[16] H. J. Park, C. H. Sohn, D. W. Jeong, G. Cao, K. W. Kim, S. J. Moon, H. Jin, D.-Y. Cho, and T. W. Noh, Phys. Rev. B **89**, 155115 (2014).
[17] H. Chu, L. Zhao, A. de la Torre, T. Hogan, S. D. Wilson, and D. Hsieh, Nat. Mater. **16**, 200 (2017).

[18] I. Nagai, Y. Yoshida, S. I. Ikeda, H. Matsuhata, H. Kito, and M. Kosaka, J. Phys. Condens. Matter **19**, 136214 (2007).
[19] S. Boseggia, R. Springell, H. C. Walker, A. T. Boothroyd, D. Prabhakaran, S. P. Collins, and D. F. McMorrow, J. Phys. Condens. Matter **24**, 312202 (2012).
[20] S. Boseggia, R. Springell, H. C. Walker, A. T. Boothroyd, D. Prabhakaran, D. Wermeille, L. Bouchenoire, S. P. Collins, and D. F. McMorrow, Phys. Rev. B **85**, 184432 (2012).
[21] C. Dhital *et al.*, Phys. Rev. B **86**, 100401(R) (2012).
[22] S. Fujiyama, K. Ohashi, H. Ohsumi, K. Sugimoto, T. Takayama, T. Komesu, M. Takata, T. Arima, and H. Takagi, Phys. Rev. B **86**, 174414 (2012).
[23] J. Kim, A. H. Said, D. Casa, M. H. Upton, T. Gog, M. Daghofer, G. Jackeli, J. van den Brink, G. Khaliullin, and B. J. Kim, Phys. Rev. Lett. **109**, 157402 (2012).
[24] J. W. Kim, Y. Choi, J. Kim, J. F. Mitchell, G. Jackeli, M. Daghofer, J. van den Brink, G. Khaliullin, and B. J. Kim, Phys. Rev. Lett. **109**, 037204 (2012).
[25] B. J. Kim *et al.*, Phys. Rev. Lett. **101**, 076402 (2008).
[26] Y. K. Kim, O. Krupin, J. D. Denlinger, A. Bostwick, E. Rotenberg, Q. Zhao, J. F. Mitchell, J. W. Allen, and B. J. Kim, Science **345**, 187 (2014).
[27] Y. K. Kim, N. H. Sung, J. D. Denlinger, and B. J. Kim, Nat. Phys. **12**, 37 (2015).
[28] L. Zhao, D. H. Torchinsky, H. Chu, V. Ivanov, R. Lifshitz, R. Flint, T. Qi, G. Cao, and D. Hsieh, Nat. Phys. **12**, 32 (2015).
[29] Y. Cao *et al.*, Nat. Commun. **7**, 11367 (2016).
[30] J. Kim *et al.*, Phys. Rev. Lett. **108**, 177003 (2012).
[31] X. Lu, D. E. McNally, M. Moretti Sala, J. Terzic, M. H. Upton, D. Casa, G. Ingold, G. Cao, and T. Schmitt, Phys. Rev. Lett. **118**, 027202 (2017).
[32] M. Moretti Sala, V. Schnells, S. Boseggia, L. Simonelli, A. Al-Zein *et al.*, Phys. Rev. B **92**, 024405 (2015).
[33] T. Hogan, R. Dally, M. Upton, J. P. Clancy, K. Finkelstein, Y.-J. Kim, M. J. Graf, and S. D. Wilson, Phys. Rev. B **94**, 100401(R) (2016).
[34] L. J. P. Ament, M. van Veenendaal, T. P. Devereaux, J. P. Hill, and J. van den Brink, Rev. Mod. Phys. **83**, 705 (2011).
[35] W. Jin *et al.*, Phys. Rev. B **99**, 041109(R) (2019).
[36] H. Gretarsson, N. H. Sung, M. Höppner, B. J. Kim, B. Keimer, and M. Le Tacon, Phys. Rev. Lett. **116**, 136401 (2016).
[37] R. R. P. Singh, P. A. Fleury, K. B. Lyons, and P. E. Sulewski, Phys. Rev. Lett. **62**, 2736 (1989).
[38] P. A. Fleury and R. Loudon, Phys. Rev. **166**, 514 (1968).
[39] J. Zhang *et al.*, npj Quantum Mater. **4**, 23 (2019).
[40] T. Hogan, L. Bjaalie, L. Zhao, C. Belvin, X. Wang, C. G. Van de Walle, D. Hsieh, and S. D. Wilson, Phys. Rev. B **93**, 134110 (2016).
[41] G. Jackeli and G. Khaliullin, Phys. Rev. Lett. **102**, 017205 (2009).
[42] See Supplemental Material at http://link.aps.org/supplemental/10.1103/PhysRevLett.125.087202 for spin-wave dispersion and two-magnon cross section calculations for a bilayer AFM, which includes Refs. [30,41,43], and [44].
[43] R. Coldea, S. M. Hayden, G. Aeppli, T. G. Perring, C. D. Frost, T. E. Mason, S. W. Cheong, and Z. Fisk, Phys. Rev. Lett. **86**, 5377 (2001).
[44] C. M. Canali and S. M. Girvin, Phys. Rev. B **45**, 7127 (1992).